Cell Reports
Medicine

Report

Broad auto-reactive IgM responses are common in critically ill patients, including those with COVID-19

Graphical abstract

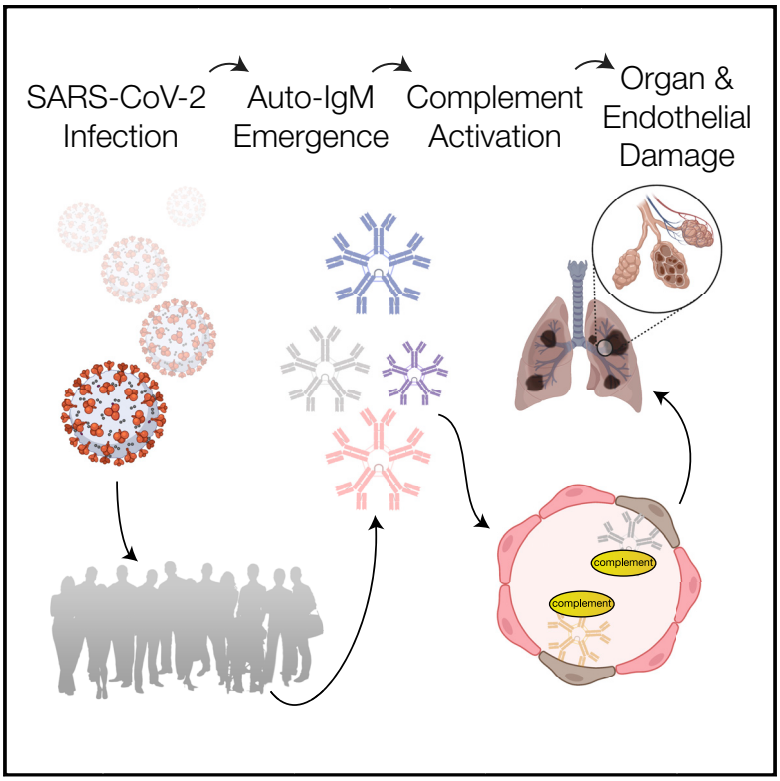

Authors

Andrew Kam Ho Wong, Isaac Woodhouse, Frank Schneider, Deanna A. Kulpa, Guido Silvestri, Cheryl L. Maier

Correspondence

cheryl.maier@emory.edu

In brief

Critical illness can be associated with immune dysregulation; yet, mediators contributing to disease severity in COVID-19 are unclear. Wong et al. show a high percentage of critically ill patients possess auto-reactive IgM, which, in SARS-CoV-2 infection, are capable of binding diverse targets across key organs and inflicting complement-dependent cytotoxicity.

Highlights

- More than 90% of critically ill COVID-19 patients have auto-reactive IgM antibodies
- Auto-reactive IgM binds diverse targets across multiple organ types
- IgM and complement component C4d are abundant in COVID-19 non-survivor lung tissue
- COVID-19-associated auto-IgM fixes complement to induce cell death *in vitro*

Wong et al., 2021, Cell Reports Medicine 2, 100321
June 15, 2021
https://doi.org/10.1016/j.xcrm.2021.100321

CellPress

Cell Reports Medicine

CellPress
OPEN ACCESS

Report

Broad auto-reactive IgM responses are common in critically ill patients, including those with COVID-19

Andrew Kam Ho Wong,[1] Isaac Woodhouse,[2] Frank Schneider,[3] Deanna A. Kulpa,[1,3] Guido Silvestri,[1,3] and Cheryl L. Maier[3,4,5,*]

[1]Emory Vaccine Center and Yerkes National Primate Research Center, Emory University, Atlanta, GA, USA
[2]Centre for Cellular and Molecular Physiology, Nuffield Department of Medicine, University of Oxford, Oxford, UK
[3]Department of Pathology and Laboratory Medicine, Emory University School of Medicine, Atlanta, GA, USA
[4]Center for Transfusion and Cellular Therapies, Emory University School of Medicine, Atlanta, GA, USA
[5]Lead contact
*Correspondence: cheryl.maier@emory.edu
https://doi.org/10.1016/j.xcrm.2021.100321

SUMMARY

The pathogenesis of severe coronavirus disease 2019 (COVID-19) remains poorly understood. While several studies suggest that immune dysregulation plays a central role, the key mediators of this process are yet to be defined. Here, we demonstrate that plasma from a high proportion (93%) of critically ill COVID-19 patients, but not healthy controls, contains broadly auto-reactive immunoglobulin M (IgM) and less frequently auto-reactive IgG or IgA. Importantly, these auto-IgMs preferentially recognize primary human lung cells *in vitro*, including pulmonary endothelial and epithelial cells. By using a combination of flow cytometry, analytical proteome microarray technology, and lactose dehydrogenase (LDH)-release cytotoxicity assays, we identify high-affinity, complement-fixing, auto-reactive IgM directed against 260 candidate autoantigens, including numerous molecules preferentially expressed on the cellular membranes of pulmonary, vascular, gastrointestinal, and renal tissues. These findings suggest that broad IgM-mediated autoimmune reactivity may be involved in the pathogenesis of severe COVID-19, thereby identifying a potential target for therapeutic interventions.

INTRODUCTION

Although severe acute respiratory syndrome coronavirus 2 (SARS-CoV-2), the etiological agent for coronavirus disease 2019 (COVID-19), is initially and preferentially tropic for respiratory cellular targets,[1–3] its pathogenetic effects can be widespread. Indeed, systemic inflammation and dysregulated hemostasis are hallmark characteristics of severe COVID-19.[4,5] The mechanisms responsible for clinical progression to severe COVID-19, which involves acute respiratory distress syndrome (ARDS)[6,7] remain poorly understood and appear to be multifactorial in nature. In this context, a relatively underexplored mechanistic pathway relates to autoimmunity. Historically, autoantibodies generated during the immune response to other infectious diseases have been observed.[8] More recently, autoantibodies that neutralize type 1 interferons were described in severe adult COVID-19,[9] as have autoantibodies against self-antigens associated with systemic lupus erythematosus and Sjögren's disease in severe pediatric COVID-19.[10] Additional reports of antiphospholipid autoantibodies have been associated with thrombotic events,[11,12] thereby linking immune dysregulation with thrombosis in severe COVID-19.[13] These observations underscore the need to closely examine the intersection of autoantibody-associated immunopathology and severe COVID-19, particularly in pulmonary and vascular sites.

RESULTS

COVID-19 patient plasma contains autoantibodies that bind diverse cell types

In this study, we first sought to detect auto-reactive antibodies in patient plasma using a comprehensive screening approach that incorporated diverse and relevant target cell types. Plasma samples were obtained from 64 patients hospitalized for COVID-19, including 55 patients with critical illness admitted to the intensive care unit (ICU; COVID ICU) and 9 patients with less severe disease admitted to the regular hospital floor (COVID non-ICU). Plasma was also obtained from 13 critically ill patients without SARS-CoV-2 infection but with pneumonia and ARDS, bacteremia, or sepsis (non-COVID ICU), 9 outpatients with hypergammaglobulinemia (Hyper-γ), and 12 healthy donors (Table S1). Samples were screened for the presence of immunoglobin M (IgM), IgG, and IgA antibodies against 5 human cell types including primary epithelial or endothelial cells of pulmonary, gut, or renal origin as well as a highly utilized immortalized cell line with a pulmonary endothelial phenotype. Given that these cells have never been exposed to SARS-CoV-2, antibodies detected in this assay reflect the targeting of self-antigens and are not the consequence of reactivity against SARS-CoV-2 antigens.

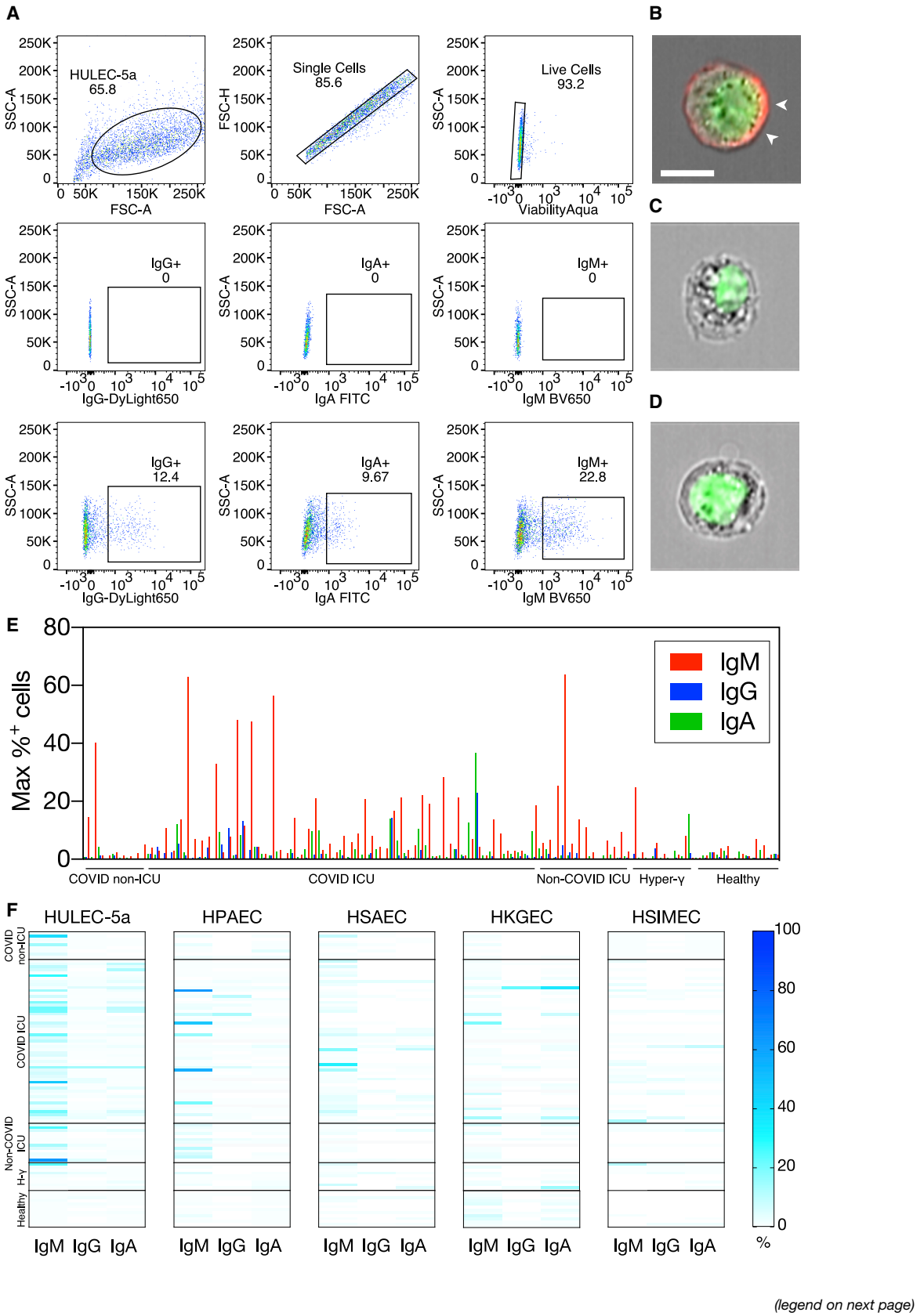

(legend on next page)

Analysis of cells using conventional (Figure 1A) and imaging flow cytometry (Figures 1B–1D) revealed the presence of antibodies binding to the plasma membrane of target cells. Scored against healthy and non-COVID controls, auto-reactive IgA, auto-reactive IgG, and auto-reactive IgM were detected in 28 (51%), 23 (42%), and 51 (93%) of 55 COVID ICU patients, respectively (Figure 1E). In each reaction, the percentage of cells that stained positively for IgM antibodies was far greater than for IgA or IgG, suggesting higher circulating auto-reactive IgM titers. Although COVID ICU patients were associated with higher circulating interleukin-6 (IL-6) and C-reactive protein (CRP) (Figures S1A and S1B), only auto-IgM levels were modestly associated with increased plasma IL-6 ($p = 0.29$, $p = 0.0056$; Figures S1D and S1D). Of note, most COVID ICU patient plasma showed IgA, IgG, IgM, or a combination of reactivity with cells of pulmonary origin (Figure 1F; Figure S1E). The presence of auto-IgM and auto-IgA antibodies in COVID ICU patients was significantly increased compared with COVID non-ICU patients and healthy controls, while increased presence of auto-IgG was suggested, but did not reach statistical significance (Figure S1G).

Inclusion of patients with non-COVID ARDS, bacteremia, or sepsis allowed for comparison of autoantibody levels in patients with critical illness from other etiologies. Similarly to what we observed in COVID ICU patients, non-COVID ICU patients had significantly increased levels of auto-IgM compared with COVID non-ICU patients and healthy controls (Figure S1E). The overall percentage of non-COVID ICU patients with auto-IgM against any of the 5 target cell types ($n = 11$; 85%; Figure S1G) was not significantly different compared with COVID ICU patients (93%; $p \geq 0.999$; Figure S1G). Nevertheless, there was a significant increase in auto-IgM directed against human small airway epithelial cells (HSAECs) when comparing COVID ICU with non-COVID ICU patient samples (Figure S1E). In addition, and despite median levels not reaching statistical significance, COVID ICU patients tended to have higher absolute levels of target cell binding to HULEC-5a and human pulmonary airway epithelial cells (HPAECs) compared with all other cohorts, including non-COVID ICU, suggesting higher auto-IgM antibody titers (Figure S1E). Interestingly, we did not find any correlation between hospitalization day and auto-IgM level in COVID ICU patient plasma (Figure S1H). Given this, as well as the higher frequency of detection and autoantibody levels, we chose to focus additional studies specifically on auto-reactive IgM. Overall, this first set of data revealed that high-titer, auto-reactive IgMs are frequently detected in critically ill patients, including those with severe COVID-19, and that the reactivity in COVID ICU patients is most pronounced against cells of pulmonary origin.

Analytical human proteome microarray reveals a broad auto-reactive IgM repertoire

We next sought to understand which autoantigens are targeted by circulating auto-reactive IgM in critically ill patients and determine whether COVID ICU patients have a distinct autoantibody profile. Samples from non-COVID ICU patients with high auto-reactive IgM levels served as important comparators to enable determination of the specificity of autoantigens present in critically ill COVID-19 patients. Thus, plasma samples with strong auto-reactive IgM titers from COVID ICU patients ($n = 5$) or non-COVID ICU patients ($n = 3$), as well as from healthy controls ($n = 4$), were surveyed in analytical human proteome microarrays (HuProt v.4 array). Each array includes more than 21,000 intact proteins, allowing for a thorough and comprehensive investigation of potential binding targets for auto-reactive IgM antibodies. For stringency, a potential binding target was considered for any protein that had a fluorescence signal at least 4 standard deviations (Z score > 4) above the array mean. Additionally, the target had to possess a fluorescence signal at least 2 Z scores above the same target across all healthy controls.

This strict approach resulted in the identification of 260 candidate autoantigens uniquely linked to COVID ICU patients (Figure 2A; Table S2). The auto-reactive IgM repertoire in COVID ICU patients was broad, and the candidate targets infrequently overlapped among different patients included in this cohort (Figure 2B), suggesting widespread immune dysregulation as opposed to a specific COVID-defining autoantibody signature. Broad auto-reactivity was also identified in the non-COVID ICU patients, consistent with the presence of auto-IgM related to critical illness rather than a distinct feature of COVID-19. It is very likely, and anticipated, that interrogation of additional plasma samples from COVID-19 patients by proteome microarray may identify further autoantigen targets. Thus, the individual antigenic targets are likely less relevant to the disease pathogenesis than the overall abundance, breadth, and tissue specificity of the observed autoantibodies.

Given the high Z scores of each candidate target, auto-reactive IgM antibodies are circulating at robust titers and/or bind with high avidity to the respective targets. We next sought to determine whether the candidate autoantigens were expressed in key tissue

Figure 1. COVID-19 patient plasma contains autoantibodies that bind diverse cell types

(A) The presence of auto-Ig was detected in human plasma by flow cytometry. Following initial gating on single and live cells (top row), populations were queried for surface-bound antibodies. Fluorescence minus one (FMO) samples (middle row) and an IgG-positive control were used to determine the IgG^+ gate (bottom left), while gates for IgA^+ and IgM^+ events were informed by FMO samples and strategic gating to restrict positive events below 2% in at least half and below 10% in all healthy donor samples (bottom middle and bottom right, respectively). Representative flow cytometry plots are shown.

(B–D) Imaging flow cytometry detected auto-IgM (pseudocolored red) bound to the plasma membrane of a human primary alveolar epithelial cell (HPAEC) stained with patient plasma containing a high level of auto-IgM (B). This was not observed in cells incubated with patient plasma without HPAEC-reactive auto-IgM (C) or with plasma obtained from a healthy human control (D). Nuclei are pseudocolored green. Scale bar, 10 μm. IgM-stained plasma membrane indicated by white arrowheads. Representative images are shown.

(E) The maximum observed auto-Ig staining percentage across all cell types, from each patient, are shown.

(F) Detected auto-Ig levels in specific cell types are shown, per patient. For (E) and (F), the ICU label designates non-COVID ICU patients; the Hyper-γ or H-γ label indicates samples from patients with hypergammaglobulinemia. Primary cells used were human kidney glomerular endothelial cells (HKGECs), human small airway epithelial cells (HSAECs), human small intestinal microvascular endothelial cells (HSIMECs), and human pulmonary airway epithelial cells (HPAECs). Because of sample constraints, each stain was performed once.

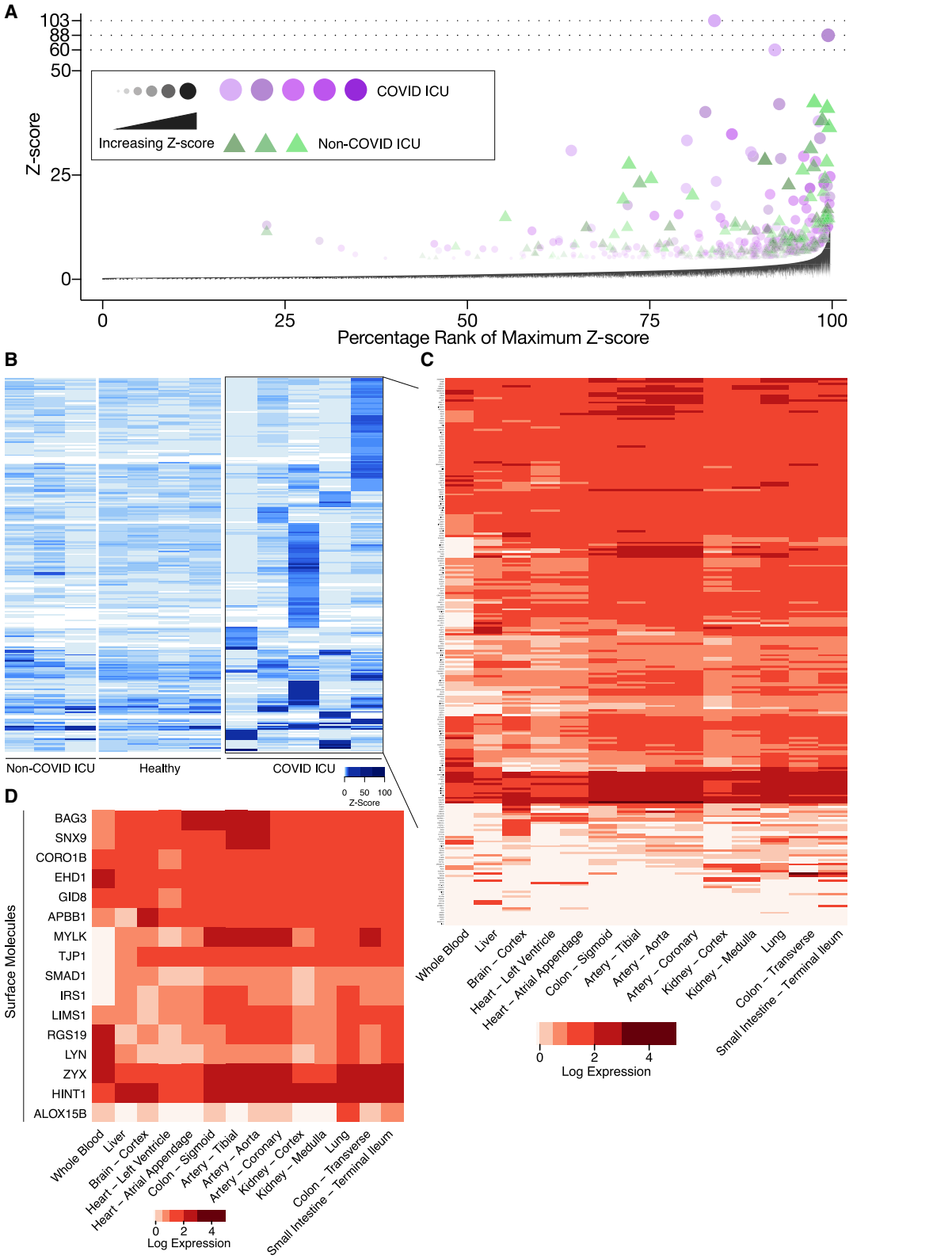

(legend on next page)

types. Using arterial tissues as surrogates for endothelialized vascular sites; small intestine and colonic tissues as surrogates for gastrointestinal sites; and renal, neural, and pulmonary sites, we found 226 candidate autoantigens expressed at above-background levels in these cell types (Figure 2C). Importantly, we identified 16 autoantigens associated with the human plasma membrane proteome[14] and therefore considered these molecules as important prospective candidate targets for circulating pathogenic auto-reactive IgM (Figure 2D). We next investigated whether these proteins shared similar motifs. Although N-linked glycosylation was predicted in 11 candidate autoantigens, heterogeneity in amino acid sequences flanking predicted N-linked glycosylated residues indicated minimal influence of N-linked glycosylation on potential IgM binding motifs (Figure S2A). However, an artificial neural network prediction model[15] revealed extensive O-linked glycosylation for 12 candidate autoantigens (Figures S2B and S2C). Notably, these sites are enriched for proline and serine, which are signs of authentic glycosylation in regions likely to mediate protein-IgM interactions.

Tissue-bound IgMs are abundant in severe COVID-19 patients and retain the ability to fix complement

The concomitant observations of auto-reactive IgM potentially targeting O-linked glycosylated motifs and high expression of candidate autoantigens in pulmonary sites led us to hypothesize that auto-reactive IgMs are a significant contributor to severe COVID-19 disease. To further explore the *in vivo* relationship between auto-reactive IgM and COVID-19 pathophysiology, we examined post-mortem pulmonary tissue to determine IgM distribution and presence in patients who died from COVID-19. Immunohistochemical staining of paraffin-embedded lung tissue revealed vastly greater IgM binding to alveolar septa and luminal surfaces of three COVID-19 non-survivors, compared to six COVID-19-negative controls (Figure 3A). The COVID-19-negative controls were selected to include post-mortem pulmonary tissue from patients with ARDS and diffuse alveolar damage (DAD; n = 3) as well as pulmonary tissue available from patients without ARDS or DAD undergoing lung cancer resection (n = 3). While we cannot formally rule out that IgMs detected in COVID-19-positive lung tissue are reactive against SARS-CoV-2 surface antigens, the observed staining patterns are not consistent with the distribution patterns observed for SARS-CoV-2 antigens such as the Spike protein.[16,17] While modest IgM staining was observed in COVID-19-negative patients, importantly, extensive IgM staining patterns were observed in COVID-19-positive patients and at levels at least three times higher ($p = 0.003$; Figure 3B) and have not been described for other causes of acute respiratory distress.[18] Histological analysis revealed significant alveolar damage and patchy hemorrhage, alongside extensive inflammatory infiltrate breaching the alveolar lumen, in the lungs of severe COVID-19 patients. Previous studies have linked alveolar damage to dysregulated cytokine release and neutrophil extracellular traps seeded by resident macrophages.[19–22] Yet, these observations could also be linked to auto-reactive IgMs through the capacity of these immunoglobulins to fix complement and induce cytotoxicity. Staining for complement component 4 (C4d), a marker of complement activation, showed a 2-fold increase in severe COVID-19 patients compared with controls ($p < 0.05$; Figure 3C), indicating frequent *in vivo* complement fixation.

Indeed, complement-dependent cytotoxicity (CDC) and complement deregulation have been proposed to play a role in the pathogenesis of ARDS.[23] Additionally, as there is considerable pulmonary microangiopathy observed in severe COVID-19 patients,[24,25] it is conceivable that CDC can precede or even cause the damage to the pulmonary endothelium. Given the observed IgM and C4d binding to pulmonary targets and to confirm that the auto-reactive IgM can mediate CDC, we next tested plasma samples from critically ill COVID-19 patients for their ability of fixing complement and inducing cytotoxicity *in vitro*. To this end, we investigated patient plasma samples, where available, that showed greater than 10% binding to the respective cell type in the screening assay. As a comparison, CDC assays were performed alongside non-COVID ICU patients samples, again where permitted by greater than 10% binding and adequate sample volumes (n = 2), given their propensity for auto-IgM detection. Interestingly, we consistently observed higher rates of CDC in cells of pulmonary origin (Figures 3D–3H). In addition, while non-COVID ICU patient plasma samples induced limited or no cell death, most COVID-19 ICU patient plasma samples induced cell death at frequencies proportional to their measured level of cell binding (Figure 3I). Collectively, these data indicate that auto-reactive IgM present in plasma from critically ill COVID-19 patients can fix complement and induce cytotoxicity.

DISCUSSION

Herein, we identify the presence of auto-reactive IgM as a common feature in critically ill patients, including those with

Figure 2. Analytical human proteome microarray reveals a broad auto-reactive IgM repertoire

(A) Plasma samples from 4 healthy human donors, alongside demonstrated auto-reactive IgM^+ plasma samples from 5 COVID ICU patients and 3 non-COVID ICU patients, were analyzed in a proteome microarray to determine potential IgM targets. *Z* score ranges (the number of standard deviations above/below the microarray signal intensity median) of targets in healthy controls were ranked in ascending order and are represented as the black trace. Candidate targets of auto-reactive IgM in patient samples were selected through possession of a 2.0 *Z* score difference compared with maximum in healthy controls, and a final *Z* score greater than 4.0. Each patient is uniquely color coded. Greater shape opacity and size indicate higher *Z* scores and are linked to higher antibody titers and/or avidity.

(B) *Z* scores of all candidate auto-reactive IgM targets (n = 260) found in COVID ICU patients are represented in this heatmap alongside *Z* scores of the corresponding target in non-COVID ICU patients and healthy human controls. The IgM repertoire of each COVID ICU patient uniquely targets a broad variety of proteins that, in turn, are generally not targeted by auto-reactive IgM found in non-COVID ICU patients and healthy controls. Key shows *Z* scores.

(C and D) Gene expression profile of candidate COVID ICU patient auto-reactive IgM targets in key organ sites shows most of the targets are normally expressed at meaningful levels (C). Heatmap representation of candidate genes empirically shown to localize at the plasma membrane and their relative expression in the listed tissue sites (D). Key shows expression levels in natural log scale.

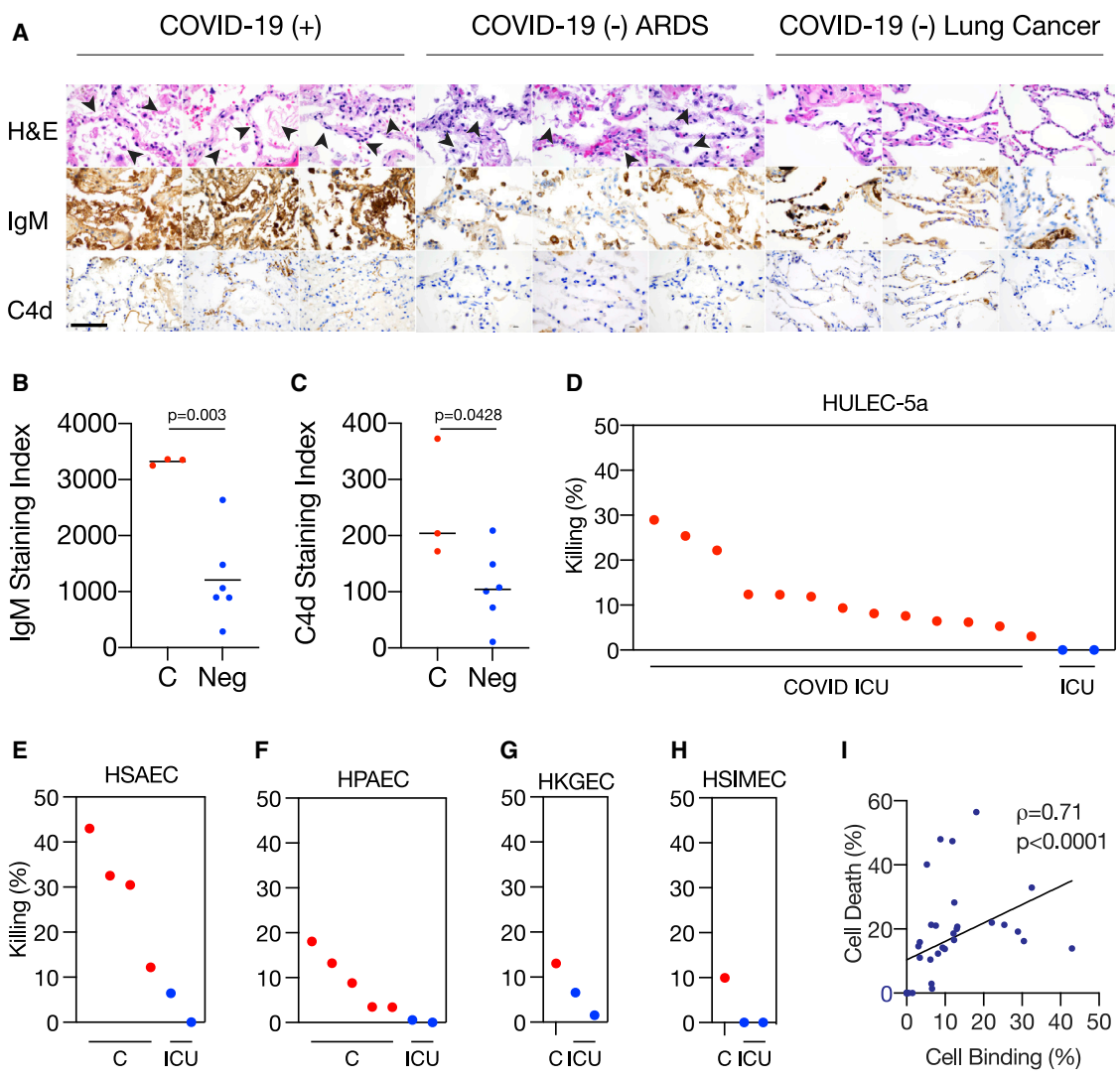

Figure 3. Tissue-bound IgMs are abundant in severe COVID-19 patients and retain the ability to fix complement

(A) Formalin-fixed, paraffin-embedded sections of lung tissue obtained from 3 COVID-19 non-survivors (left), 3 COVID-19-negative non-survivors with acute respiratory distress syndrome (ARDS) and diffuse alveolar damage (DAD; middle), and 3 COVID-19-negative lung cancer resection patients (right) were prepared with a hematoxylin and eosin stain (H&E) or probed for IgM and C4d. Substantial infiltration of the alveolar lumina and disruption of alveolar septa were observed in sections from COVID-19 and non-COVID ARDS lungs (indicated by black arrowheads). Black distance bar: 100 μm (H&E and IgM) and 500 μm (C4d).

(B and C) Lung sections in (A) of COVID-19 non-survivors ("C") were associated with higher staining indices for IgM (B) and C4d (C) compared with the non-COVID controls (Neg), which signal greater presence of IgM and C4d in lung sites. Staining indices were calculated by dividing the total area stained per image by the number of nuclei present. Horizontal bars represent mean. Statistical significances were determined by a two-tailed t test.

(D–H) Patients admitted to the ICU for COVID-19 (depicted under "C" or COVID ICU) whose plasma samples demonstrated high levels of auto-reactive IgM were screened on pulmonary endothelia (D) bronchial epithelia (E), alveolar epithelia (F), renal endothelia (G), and small intestinal epithelia (H). The addition of purified rabbit complement demonstrated that auto-reactive IgM from COVID-19 ICU patients retained complement-fixing capabilities and could induce cytotoxicity, as measured by lactose dehydrogenase (LDH) release. By contrast, plasma samples from non-COVID ICU patients (ICU) exhibited minimal complement-fixing capacity.

(I) The frequency of cell death following complement fixation correlates with the magnitude of IgM binding, as determined previously by flow cytometry. Correlation was determined by a two-tailed Spearman test. LDH release assays were performed once per patient per cell type, given highly limited availability of test sample.

COVID-19. These auto-IgMs have broad reactivity, and while they are significantly increased in critically ill versus non-critically ill COVID patients, they are not necessarily a unique feature of COVID, as non-COVID ICU patients also demonstrated a high prevalence of auto-IgM in our study. Nevertheless, auto-IgM directed against certain human pulmonary epithelial cells was significantly increased in COVID ICU patients compared with non-COVID ICU patients and was capable of fixing complement and inducing target cell death *in vitro*.

The identification of auto-reactive IgM as a potential contributing factor to the pathogenesis of severe COVID-19 has two immediate implications. First, this observation may explain how COVID-19 is disproportionately more serious in the elderly,[26] who typically manifest higher plasma levels of circulating auto-reactive antibodies.[27] This phenomenon would be exacerbated by decreases in functional T follicular helper cells that promote antibody class switching,[28] a process associated with better disease outcomes.[29] Given that IgM levels peak within a week of the clinical onset of COVID-19 and persist at similar levels for weeks thereafter,[30,31] the elderly face a protracted period where there may be steadfast secretion of auto-reactive IgM that maintains relatively low affinity for the same epitope without either switching to alternate antibody class types or undergoing somatic hypermutation and affinity maturation. In this perspective, the elderly may be more prone to severe COVID-19 due to a more protracted exposure to the cytopathic effects of auto-reactive IgM.

Second, it is conceivable that this type of immunopathology can be limited by therapeutic interventions that inhibit the IgM-complement axis. In the immediate term, this approach could mitigate the SARS-CoV-2-associated alveolar damage and ARDS[32–34] and consequently protect against mortality[35] and/or reduce the need for invasive mechanical ventilation.[36] In the longer term, preservation of lung integrity may prevent pathogenic sequelae such as pulmonary fibrosis,[37,38] which diminishes lung function post-recovery.[39] These therapeutic goals could be implemented through the use of immunosuppressants, such as dexamethasone, that can attenuate the production of auto-reactive IgM,[40] plasma exchange to remove auto-reactive IgM once formed[41,42] or to synergize and supplement proposed anti-fibrotic therapies.[43] While dexamethasone has been widely utilized in COVID-19, its role in suppressing an autoantibody response is not yet clear and future studies should directly investigate the effect of corticosteroids on autoantibody responses and patient outcomes. Alternatively, the complement cascade can be directly inhibited through conestat alfa[44] or eculizumab;[45] indeed, both drugs are presently undergoing evaluation through clinical trials to determine efficacy.[45] Optimistically, our findings cast support for interventions that can be readily and swiftly implemented in the clinic to alleviate or prevent serious COVID-19 complications.

In summary, we found that broadly auto-reactive IgMs are common in the plasma of critically ill patients such as those with COVID-19. These auto-reactive antibodies bind pulmonary epithelial and endothelial targets at which point they can be potent mediators of cytopathicity through the recruitment of complement. Future studies will investigate the relationship between SARS-CoV-2 infection and the emergence and kinetics of auto-reactive antibodies and determine whether immunosuppressive therapy can reduce the levels of auto-reactive IgM in plasma and consequently attenuate the clinical severity of COVID-19.

Limitations of the study

It is important to note several major limitations of our study. The use of residual clinical samples available from COVID-19 patients at only a single time point severely curtailed our ability for additional analyses, such as determining total IgG, IgA, and IgM levels, following the time course of autoantibody generation and contraction, or characterizing cellular components involved in antibody production such as plasmablasts. At this juncture, we cannot conclude that auto-reactivity is unique to or causative of severe COVID-19, and certainly generation of autoantibodies may be relevant to the pathophysiology of other infectious diseases. A paucity of cases of other respiratory illnesses associated with ARDS, such as influenza, precluded our ability to characterize the full extent to which auto-reactive antibodies are present and/or function in relation to other severe diseases. Future studies from prospectively enrolled patients, including those with influenza or other respiratory illnesses, will be essential for resolving this and will also provide clarity on the timing of autoantibody generation and contraction during the course of acute disease in patients with COVID-19.

STAR★METHODS

Detailed methods are provided in the online version of this paper and include the following:

- KEY RESOURCES TABLE
- RESOURCE AVAILABILITY
  - Materials availability
- EXPERIMENTAL MODEL AND SUBJECT DETAILS
  - Plasma samples
  - Cells
- METHOD DETAILS
  - Flow cytometry detection of auto-antibodies
  - IL-6 ELISA
  - Histology
  - Complement fixing assay
  - Protein array
  - Gene expression analysis
- QUANTIFICATION AND STATISTICAL ANALYSIS

SUPPLEMENTAL INFORMATION

Supplemental information can be found online at https://doi.org/10.1016/j.xcrm.2021.100321.

ACKNOWLEDGMENTS

The authors wish to acknowledge the members of Emory's COVID-19 Anticoagulation Working Group, led by Sara C. Auld, as well as the clinical and laboratory staff caring for these patients. C.L.M. is supported by NIH/NHLBI K99 HL150626-01. Research reported in this publication was supported, in part, by the Pediatrics/Winship Flow Cytometry Core of Winship Cancer Institute of Emory University, Children's Healthcare of Atlanta, and NIH/NCI under award P30CA138292. The content is solely the responsibility of the authors and does not necessarily represent the official views of the National Institutes of Health. Antigen-specificity screening services were performed on HuProt v.4.0 proteome microarrays by CDI Laboratories, Antygen Division (Baltimore, MD). HuProt arrays contain >21,000 unique full-length recombinant human proteins expressed in yeast and purified with glutathione S-transferase (GST)-tags. The graphical abstract was generated using BioRender.com.

AUTHOR CONTRIBUTIONS

A.K.H.W., D.A.K., G.S., and C.L.M. conceived and designed the study. A.K.H.W. performed the experiments. I.W. performed all bioinformatic analyses. F.S. performed all histology. A.K.H.W. wrote the initial manuscript, which was reviewed and commented on by all authors. C.L.M. served as the principal investigator.

DECLARATION OF INTERESTS

The authors declare no competing interests.

Received: February 4, 2021
Revised: April 9, 2021
Accepted: May 20, 2021
Published: May 28, 2021

REFERENCES

1. Puelles, V.G., Lütgehetmann, M., Lindenmeyer, M.T., Sperhake, J.P., Wong, M.N., Allweiss, L., Chilla, S., Heinemann, A., Wanner, N., Liu, S., et al. (2020). Multiorgan and Renal Tropism of SARS-CoV-2. N. Engl. J. Med. *383*, 590–592.
2. Zou, L., Ruan, F., Huang, M., Liang, L., Huang, H., Hong, Z., Yu, J., Kang, M., Song, Y., Xia, J., et al. (2020). SARS-CoV-2 Viral Load in Upper Respiratory Specimens of Infected Patients. N. Engl. J. Med. *382*, 1177–1179.
3. Martines, R.B., Ritter, J.M., Matkovic, E., Gary, J., Bollweg, B.C., Bullock, H., Goldsmith, C.S., Silva-Flannery, L., Seixas, J.N., Reagan-Steiner, S., et al. (2020). Pathology and Pathogenesis of SARS-CoV-2 Associated with Fatal Coronavirus Disease, United States. Emerg. Infect. Dis. *26*, 2005–2015.
4. García, L.F. (2020). Immune Response, Inflammation, and the Clinical Spectrum of COVID-19. Front. Immunol. *11*, 1441.
5. Colling, M.E., and Kanthi, Y. (2020). COVID-19-associated coagulopathy: An exploration of mechanisms. Vasc. Med. *25*, 471–478.
6. Berlin, D.A., Gulick, R.M., and Martinez, F.J. (2020). Severe Covid-19. N. Engl. J. Med. *383*, 2451–2460.
7. Huang, A.T., Garcia-Carreras, B., Hitchings, M.D.T., Yang, B., Katzelnick, L.C., Rattigan, S.M., Borgert, B.A., Moreno, C.A., Solomon, B.D., Trimmer-Smith, L., et al. (2020). A systematic review of antibody mediated immunity to coronaviruses: kinetics, correlates of protection, and association with severity. Nat. Commun. *11*, 4704.
8. Ikematsu, H., Harindranath, N., Ueki, Y., Notkins, A.L., and Casali, P. (1993). Clonal analysis of a human antibody response. II. Sequences of the VH genes of human IgM, IgG, and IgA to rabies virus reveal preferential utilization of VHIII segments and somatic hypermutation. J. Immunol. *150*, 1325–1337.
9. Bastard, P., Rosen, L.B., Zhang, Q., Michailidis, E., Hoffmann, H.-H., Zhang, Y., Dorgham, K., Philippot, Q., Rosain, J., Béziat, V., et al. (2020). Autoantibodies against type I IFNs in patients with life-threatening COVID-19. Science *370*, eabd4585.
10. Gruber, C.N., Patel, R.S., Trachtman, R., Lepow, L., Amanat, F., Krammer, F., Wilson, K.M., Onel, K., Geanon, D., Tuballes, K., et al. (2020). Mapping Systemic Inflammation and Antibody Responses in Multisystem Inflammatory Syndrome in Children (MIS-C). Cell *183*, 982–995.e14.
11. Xiao, M., Zhang, Y., Zhang, S., Qin, X., Xia, P., Cao, W., Jiang, W., Chen, H., Ding, X., Zhao, H., et al. (2020). Antiphospholipid Antibodies in Critically Ill Patients With COVID-19. Arthritis Rheumatol. *72*, 1998–2004.
12. Zuo, Y., Estes, S.K., Ali, R.A., Gandhi, A.A., Yalavarthi, S., Shi, H., Sule, G., Gockman, K., Madison, J.A., Zuo, M., et al. (2020). Prothrombotic autoantibodies in serum from patients hospitalized with COVID-19. Sci. Transl. Med. *12*, eabd3876.
13. Patel, B.V., Arachchillage, D.J., Ridge, C.A., Bianchi, P., Doyle, J.F., Garfield, B., Ledot, S., Morgan, C., Passariello, M., Price, S., et al. (2020). Pulmonary Angiopathy in Severe COVID-19: Physiologic, Imaging, and Hematologic Observations. Am. J. Respir. Crit. Care Med. *202*, 690–699.
14. Uhlén, M., Fagerberg, L., Hallström, B.M., Lindskog, C., Oksvold, P., Mardinoglu, A., Sivertsson, Å., Kampf, C., Sjöstedt, E., Asplund, A., et al. (2015). Proteomics. Tissue-based map of the human proteome. Science *347*, 1260419.
15. Gupta, R., and Brunak, S. (2002). Prediction of glycosylation across the human proteome and the correlation to protein function. Pac. Symp. Biocomput. 310–322.
16. Bradley, B.T., Maioli, H., Johnston, R., Chaudhry, I., Fink, S.L., Xu, H., Najafian, B., Deutsch, G., Lacy, J.M., Williams, T., et al. (2020). Histopathology and ultrastructural findings of fatal COVID-19 infections in Washington State: a case series. Lancet *396*, 320–332.
17. Borczuk, A.C., Salvatore, S.P., Seshan, S.V., Patel, S.S., Bussel, J.B., Mostyka, M., Elsoukkary, S., He, B., Del Vecchio, C., Fortarezza, F., et al. (2020). COVID-19 pulmonary pathology: a multi-institutional autopsy cohort from Italy and New York City. Mod. Pathol. *33*, 2156–2168.
18. Herrero, R., Sanchez, G., and Lorente, J.A. (2018). New insights into the mechanisms of pulmonary edema in acute lung injury. Ann. Transl. Med. *6*, 32–32.
19. Hoang, T.N., Pino, M., Boddapati, A.K., Viox, E.G., Starke, C.E., Upadhyay, A.A., et al. (2020). Baricitinib treatment resolves lower airway macrophage inflammation and neutrophil recruitment in SARS-CoV-2-infected rhesus macaques. Cell *184*, 460–475.e21.
20. Wilson, M.S., and Wynn, T.A. (2009). Pulmonary fibrosis: pathogenesis, etiology and regulation. Mucosal Immunol. *2*, 103–121.
21. Middleton, E.A., He, X.-Y., Denorme, F., Campbell, R.A., Ng, D., Salvatore, S.P., Mostyka, M., Baxter-Stoltzfus, A., Borczuk, A.C., Loda, M., et al. (2020). Neutrophil extracellular traps contribute to immunothrombosis in COVID-19 acute respiratory distress syndrome. Blood *136*, 1169–1179.
22. McGonagle, D., O'Donnell, J.S., Sharif, K., Emery, P., and Bridgewood, C. (2020). Immune mechanisms of pulmonary intravascular coagulopathy in COVID-19 pneumonia. Lancet Rheumatol. *2*, e437–e445.
23. Risitano, A.M., Mastellos, D.C., Huber-Lang, M., Yancopoulou, D., Garlanda, C., Ciceri, F., and Lambris, J.D. (2020). Complement as a target in COVID-19? Nat. Rev. Immunol. *20*, 343–344.
24. Wichmann, D., Sperhake, J.-P., Lütgehetmann, M., Steurer, S., Edler, C., Heinemann, A., Heinrich, F., Mushumba, H., Kniep, I., Schröder, A.S., et al. (2020). Autopsy Findings and Venous Thromboembolism in Patients With COVID-19: A Prospective Cohort Study. Ann. Intern. Med. *173*, 268–277.
25. Lucatelli, P., Monte, M.D., Rubeis, G.D., Cundari, G., Francone, M., Panebianco, V., et al. (2020). Did we turn a blind eye? The answer is simply there. Peripheral pulmonary vascular thrombosis in COVID-19 patients explains sudden worsening of clinical conditions. Imaging *12*, 4–7.
26. Onder, G., Rezza, G., and Brusaferro, S. (2020). Case-Fatality Rate and Characteristics of Patients Dying in Relation to COVID-19 in Italy. JAMA *323*, 1775–1776.
27. Ma, S., Wang, C., Mao, X., and Hao, Y. (2019). B Cell Dysfunction Associated With Aging and Autoimmune Diseases. Front. Immunol. *10*, 318.
28. Linterman, M.A. (2014). How T follicular helper cells and the germinal centre response change with age. Immunol. Cell Biol. *92*, 72–79.
29. Zohar, T., Loos, C., Fischinger, S., Atyeo, C., Wang, C., Slein, M.D., Burke, J., Yu, J., Feldman, J., Hauser, B.M., et al. (2020). Compromised humoral functional evolution tracks with SARS-CoV-2 mortality. Cell *183*, 1508–1519.e12.
30. Ma, H., Zeng, W., He, H., Zhao, D., Jiang, D., Zhou, P., Cheng, L., Li, Y., Ma, X., and Jin, T. (2020). Serum IgA, IgM, and IgG responses in COVID-19. Cell. Mol. Immunol. *17*, 773–775.
31. Hayakawa, K., Asano, M., Shinton, S.A., Gui, M., Allman, D., Stewart, C.L., Silver, J., and Hardy, R.R. (1999). Positive selection of natural autoreactive B cells. Science *285*, 113–116.
32. Cardinal-Fernández, P., Lorente, J.A., Ballén-Barragán, A., and Matute-Bello, G. (2017). Acute Respiratory Distress Syndrome and Diffuse

Alveolar Damage. New Insights on a Complex Relationship. Ann. Am. Thorac. Soc. *14*, 844–850.

33. Castro, C.Y. (2006). ARDS and diffuse alveolar damage: a pathologist's perspective. Semin. Thorac. Cardiovasc. Surg. *18*, 13–19.
34. Mortelliti, M.P., and Manning, H.L. (2002). Acute respiratory distress syndrome. Am. Fam. Physician *65*, 1823–1830.
35. Tzotzos, S.J., Fischer, B., Fischer, H., and Zeitlinger, M. (2020). Incidence of ARDS and outcomes in hospitalized patients with COVID-19: a global literature survey. Crit. Care *24*, 516.
36. Hernandez-Romieu, A.C., Adelman, M.W., Hockstein, M.A., Robichaux, C.J., Edwards, J.A., Fazio, J.C., Blum, J.M., Jabaley, C.S., Caridi-Scheible, M., Martin, G.S., et al. (2020). Timing of Intubation and Mortality Among Critically Ill Coronavirus Disease 2019 Patients: A Single-Center Cohort Study. Crit. Care Med. *48*, e1045–e1053.
37. Fraser, E. (2020). Long term respiratory complications of covid-19. BMJ *370*, m3001.
38. Spagnolo, P., Balestro, E., Aliberti, S., Cocconcelli, E., Biondini, D., Casa, G.D., Sverzellati, N., and Maher, T.M. (2020). Pulmonary fibrosis secondary to COVID-19: a call to arms? Lancet Respir. Med. *8*, 750–752.
39. Gentile, F., Aimo, A., Forfori, F., Catapano, G., Clemente, A., Cademartiri, F., Emdin, M., and Giannoni, A. (2020). COVID-19 and risk of pulmonary fibrosis: the importance of planning ahead. Eur. J. Prev. Cardiol. *27*, 1442–1446.
40. Bos, W.H., Dijkmans, B.A.C., Boers, M., van de Stadt, R.J., and van Schaardenburg, D. (2010). Effect of dexamethasone on autoantibody levels and arthritis development in patients with arthralgia: a randomised trial. Ann. Rheum. Dis. *69*, 571–574.
41. Truong, A.D., Auld, S.C., Barker, N.A., Friend, S., Wynn, A.T., Cobb, J., et al. (2020). Therapeutic plasma exchange for COVID-19-associated hyperviscosity. Transfusion *61*, 1029–1034.
42. Maier, C.L., Truong, A.D., Auld, S.C., Polly, D.M., Tanksley, C.-L., and Duncan, A. (2020). COVID-19-associated hyperviscosity: a link between inflammation and thrombophilia? Lancet *395*, 1758–1759.
43. George, P.M., Wells, A.U., and Jenkins, R.G. (2020). Pulmonary fibrosis and COVID-19: the potential role for antifibrotic therapy. Lancet Respir. Med. *8*, 807–815.
44. Urwyler, P., Moser, S., Charitos, P., Heijnen, I.A.F.M., Rudin, M., Sommer, G., Giannetti, B.M., Bassetti, S., Sendi, P., Trendelenburg, M., and Osthoff, M. (2020). Treatment of COVID-19 With Conestat Alfa, a Regulator of the Complement, Contact Activation and Kallikrein-Kinin System. Front. Immunol. *11*, 2072.
45. Ortiz, A. (2020). Complement and protection from tissue injury in COVID-19. Clin. Kidney J. *13*, 734–738.
46. Steentoft, C., Vakhrushev, S.Y., Joshi, H.J., Kong, Y., Vester-Christensen, M.B., Schjoldager, K.T.G., Lavrsen, K., Dabelsteen, S., Pedersen, N.B., Marcos-Silva, L., et al. (2013). Precision mapping of the human O-GalNAc glycoproteome through SimpleCell technology. EMBO J. *32*, 1478–1488.

STAR★METHODS

KEY RESOURCES TABLE

REAGENT or RESOURCE	SOURCE	IDENTIFIER
Antibodies		
Rabbit anti-human IgM	Agilent	Cat# F0203; RRID:AB_2335711
Rabbit anti-C4d	ALPCO Diagnostics	Cat# 04-BI-RC4D; RRID:AB_829387
Human anti-CD98	Absolute Antibody	Ab00361-10.0
Mouse anti-CD62E BV605	Becton Dickinson	Cat# 563359; RRID: AB_2738156
Mouse anti-CD54 BV711	Becton Dickinson	Cat# 564078; RRID:AB_2738579
Mouse anti-CD144 BV786	Becton Dickinson	Cat# 565672; RRID:AB_2739327
Mouse anti-CD31 PE	Becton Dickinson	Cat# 555446; RRID:AB_395839
Goat anti-Human IgG DyLight 650	ThermoFisher	Cat# SA5-10137; RRID:AB_2556717
Goat anti-Human IgA FITC	ThermoFisher	Cat# A18788; RRID:AB_2535565
Mouse anti-Human IgM BV650	BioLegend	Cat# 314526; RRID:AB_2563836
Biological samples		
COVID non-ICU patient plasma	This paper	N/A
COVID ICU patient plasma	This paper	N/A
Non-COVID ICU patient plasma	This paper	N/A
Hyper gammaglobulinemic patient plasma	This paper	N/A
Healthy patient plasma	This paper	N/A
Chemicals, peptides, and recombinant proteins		
Rabbit complement	Cedarlane	CL3051
Critical commercial assays		
Lactose Dehydrogenase Assay	ThermoFisher	C20301
Human IL-6 ELISA	Abcam	ab178013
Deposited data		
Patient autoIgM screen on HuProt	This paper; Mendeley Data	https://dx.doi.org/10.17632/k33vwbdfsn.3
Experimental models: Cell lines		
HULEC-5a	ATCC	CRL-3244
Human Small Airway Epithelial Cells	Lifeline Cell Technology	FC-0016
Human Alveolar Epithelial Cells	CellBiologics	H-6053
Human Kidney Glomerular Endothelial cells	CellBiologics	H-6014G
Human Small Intestine Microvascular Endothelial Cells	Neuromics	HEC15
Software and algorithms		
FlowJo 10	Becton Dickinson	https://www.flowjo.com/
Prism 9	Graphpad	https://www.graphpad.com/
RStudio Desktop 1.3	RStudio PBC	https://www.rstudio.com/
NetNGlyc	Technical University of Denmark	www.cbs.dtu.dk/services/NetNGlyc/
YinOYang	Technical University of Denmark	www.cbs.dtu.dk/services/YinOYang/

RESOURCE AVAILABILITY

Additional reasonable requests for information should be directed to the lead contact, Cheryl Maier (cheryl.maier@emory.edu).

Materials availability

No unique materials were generated in the preparation of this manuscript.

EXPERIMENTAL MODEL AND SUBJECT DETAILS

Plasma samples

Residual plasma samples were collected after clinical testing from patients admitted to an Emory Healthcare facility (i.e., ''discarded clinical specimens'') or from healthy donors in accordance with protocols approved by Emory's Institutional Review Board. Patient demographics and characteristics were obtained by electronic chart review as summarized in Table S1. C-Reactive Protein levels were determined during routine hospital care and reported where available.

Cells

HULEC-5a cells were obtained from the American Type Culture Collection (ATCC) and maintained in MCDB131 Medium (GIBCO, Thermo Fisher) supplemented with 10ng/ml epidermal growth factor (Thermo Fisher), 1μg/ml hydrocortisone (Sigma Aldrich), 10mM L-glutamine (Thermo Fisher), and 10% (v/v) FCS (GeminiBio). Primary human small airway epithelial cells (HSAEC) were purchased (Lifeline Cell Technology) and maintained in BronchiaLife Medium (cat. no. LKL-0023, Lifeline Cell Technology). Primary human alveolar epithelial cells (HAEC) and primary human kidney glomerular endothelial cells (HKGEC) were purchased (CellBiologics) and maintained in Complete Human Epithelial Cell Medium (cat. no. H6621, CellBiologics) and Complete Human Endothelial Cell Medium (cat. no. H1168, CellBiologics), respectively. Primary human small intestine microvascular endothelial cells were purchased (Neuromics) and maintained in ENDO-Growth Medium (cat. no. EGK001, Neuromics). All cells were kept at 37°C in a humidified incubator supplemented with 5% CO_2 and maintained between 50%–80% confluence. Primary cells were grown in cell culture flasks coated with gelatin (cat. no. 6950, CellBiologics) and used between 3-7 passages.

METHOD DETAILS

Flow cytometry detection of auto-antibodies

Plasma aliquots were stored at −80°C and then thawed at 4°C for use in assays. Cells were detached from culture flasks using TrypLE Express reagent (Thermo Fisher) and resuspended in DPBS at a concentration of $5x10^5$ cells/ml. 100μl of each cell suspension was added to 96-well U-bottom plates, and 50μl of patient or healthy donor plasma added and gently mixed. An IgG positive control was performed by adding human anti-CD98 IgG (cat. no. Ab00361-10.0, Absolute Antibody, 2μl) to one well. Plates were transferred to 4°C for one hour, after which cells were washed with cold DPBS and then incubated with an antibody cocktail containing a viability dye (LIVE/DEAD Aqua, Thermo Fisher), anti-CD62E BV605 (cat. no., 563359, BD, 2.5μl), anti-CD54 BV711 (cat. no., 564078, BD, 2.5μl), anti-CD144 BV786 (cat. no., 565672, BD, 2.5μl), anti-CD31 PE (cat. no., 555446, BD, 10μl), anti-human IgG DyLight 650 (cat. no., SA5-10137, Thermo Fisher, 2μl), anti-human IgA FITC (cat. no., A18788, Thermo Fisher, 0.1μl) and anti-human IgM BV650 (cat. no., BioLegend, 314526, 2μl). No-anti-Ig fluorescence minus one controls were also prepared. After one hour at 4°C, cells were washed twice with FACS buffer and then fixed with 1% PFA before analysis on a BD LSRFortessa flow cytometer. For imaging flow cytometry, cells were stained only with anti-IgM BV650 following plasma incubation. Nuclei were stained with NucSpot Live 488 (cat. no. 40081, Biotium, 1:1000). Cells were then fixed in 2% PFA and analyzed on a Luminex Amnis ImageStreamX Mark II flow cytometer.

IL-6 ELISA

Plasma levels of IL-6 were quantified using a Human IL-6 ELISA kit (ab178013, Abcam) and following the manufacturer's instructions.

Histology

Five-micrometer sections from formalin-fixed, paraffin-embedded lung tissue sections were tested for IgM expression using a rabbit anti-IgM polyclonal antibody (cat. no. F0203, Agilent, Santa Clara, CA) at 1:400 dilution and for C4d expression using a rabbit anti-C4d polyclonal antibody (cat. no. 04-BI-RC4D, ALPCO Diagnostics, Salem, NH) at 1:100 dilution. IgM staining was performed on a Dako Link48 Autostainer with the EnVision FLEX dual-link system (Dako, Carpinteria, California) after heat-induced epitope retrieval in citrate buffer for 30 minutes. C4d staining was performed on a Leica Bond III automated stainer with the Bond Polymer Refine Detection Kit (Leica Microsystems, Bannockburn, IL) after on-board epitope retrieval using Bond epitope retrieval solution 1 (ER1) for 20 minutes. Images were analyzed in ImageJ using the IHC Image Analysis Toolbox for the enumeration of nuclei, and to identify stained regions. The Color Pixel Counter plugin was further used to quantify the extent of staining in each image.

Complement fixing assay

Target cells were dissociated from culture flasks by TrypLE Express reagent (GIBCO) and resuspended in PBS at a concentration of $1x10^6$ cells/ml. 50μl of the cell suspension was transferred to wells of a 96-well V-bottom plate. 50μl of plasma was added to each well and plates were incubated at 4°C for one hour. Limited samples regrettably imposed constraints that meant only 2 non-COVID (ICU) samples with high IgM reactivity and 2 healthy donor plasma samples without IgM reactivity could be consistently utilized herein as

controls. Cells were washed with cold DPBS twice and resuspended in 100μl DPBS. 11μl of reconstituted rabbit complement (Low-Tox-M rabbit complement, Cedarlane) was added to each well. To one well, 0.1% Triton X-100 was added to induce cell lysis. Plates were then transferred to a 37°C incubator for two hours. Plates were then centrifuged at 500 g for 5 minutes to pellet cells. 50μl of the supernatant was transferred to a flat-bottom 96-well plate in duplicate. 50μl of reconstituted lactose dehydrogenase assay reagent (CyQUANT LDH Cytotoxicity Assay, Invitrogen) was then added to each well, and the plate was subsequently protected from light and left at ambient temperature for 30 minutes, after which 50μl of the included stop solution was added. Absorbance was read at 490nm and 680nm (Varioskan LUX multimode plate reader, Thermo Fisher). Absorbance values at 680nm were subtracted from absorbances at 490nm and duplicate values averaged. Percentage cytotoxicity was calculated by comparing the absorbance values against the lysed-cell and healthy-donor controls.

Protein array

5 COVID-19 (ICU) and 3 non-COVID-19 (ICU) samples characterized as enriched with auto-IgM by the flow cytometry assay described above were submitted alongside 4 randomly chosen healthy control samples to CDI laboratories (Baltimore, MD) for antigen-specificity screening across > 21,000 full-length recombinant human protein targets (HuProt v4.0 proteome microarray). These microarrays screened the same input volume of neat plasma, diluted 1:1000 per patient, to allow for an estimation of auto-Ig levels across multiple patients. Detection of IgM was made via a secondary antibody.

Gene expression analysis

Tissue-level transcription profiles were based on the Transcript TPMs dataset provided by the GTEx Portal. Subcellular localization data provided by the Human Protein Atlas[14] guided the identification of plasma membrane proteins. For all analyses, plasma membrane proteins were those defined as 'Enhanced' or 'Supported' for plasma membrane localization. Visualizations and heatmaps were generated with GraphPad Prism (v9.0) and RStudio Desktop (1.3.959). Predictions of N- and O-linked glycosylated sites were respectively provided by NetNGlyc[46] and YinOYang servers,[15] and only high-cutoff sites were chosen for further analysis. Amino acid probability graphs were generated with WebLogo 3.

QUANTIFICATION AND STATISTICAL ANALYSIS

GraphPad Prism (v9.0) was used to calculate statistical significances and correlations. Corresponding statistical tests are noted in figure legends.